



**HAL**  
open science

# A Graded Index All-Dielectric Lens for Field Decorrelation and Decoupling of a Wideband MIMO Antenna

Usman Qureshi, Muhammad Umar Khan, Mohammad Sharawi, Shah Nawaz Burokur, Raj Mittra

► **To cite this version:**

Usman Qureshi, Muhammad Umar Khan, Mohammad Sharawi, Shah Nawaz Burokur, Raj Mittra. A Graded Index All-Dielectric Lens for Field Decorrelation and Decoupling of a Wideband MIMO Antenna. IEEE Open Journal of Antennas and Propagation, 2023, 4, pp.180-195. 10.1109/OJAP.2023.3241349 . hal-04214255

**HAL Id: hal-04214255**

**<https://hal.parisnanterre.fr/hal-04214255>**

Submitted on 15 Jan 2024

**HAL** is a multi-disciplinary open access archive for the deposit and dissemination of scientific research documents, whether they are published or not. The documents may come from teaching and research institutions in France or abroad, or from public or private research centers.

L'archive ouverte pluridisciplinaire **HAL**, est destinée au dépôt et à la diffusion de documents scientifiques de niveau recherche, publiés ou non, émanant des établissements d'enseignement et de recherche français ou étrangers, des laboratoires publics ou privés.

# A Graded Index All-Dielectric Lens for Field Decorrelation and Decoupling of a Wideband MIMO Antenna

USMAN QURESHI<sup>1</sup>, MUHAMMAD U. KHAN<sup>1</sup> (Member, IEEE), MOHAMMAD S. SHARAWI<sup>2</sup> (Senior Member, IEEE), SHAH NAWAZ BUROKUR<sup>3</sup> (Senior Member, IEEE) and RAJ MITTRA<sup>4</sup> (Life Fellow, IEEE)

<sup>1</sup>School of Electrical Engineering & Computer Science (SEecs), National University of Sciences and Technology, Islamabad 44000, Pakistan

<sup>2</sup>Department of Electrical Engineering, Polytechnique Montréal, Montréal, QC H3T 1J4, Canada

<sup>3</sup>LEME, UPL, Univ Paris Nanterre, F92410 Ville d'Avray, France

<sup>4</sup>Department of Electrical and Computer Engineering, University of Central Florida, FL 32816, USA and also with the King AbdulAziz University (KAU), Jeddah, Saudi Arabia.

CORRESPONDING AUTHOR: U. Qureshi (e-mail: uqureshi.msee17seecs@seecs.edu.pk).

**ABSTRACT** In this paper a broadband graded index all-dielectric (GID) lens that enables field decorrelation and decoupling of closely spaced wideband multiple-input-multiple-output (MIMO) antenna elements, is presented. Reduction in correlation coefficient  $\rho$  for field decorrelation and port decoupling is realized by tilting the individual antenna element radiation patterns away from each other and by suppressing the surface wave propagation inside the antenna substrate through judicious control of the permittivity profile of the GID lens using the concept of transformation electromagnetics (TE). The permittivity profile of the GID lens is designed using air-hole technology and is fabricated by additive manufacturing. To validate the proposed concept, six different examples of lens loaded wideband patch-based MIMO antenna elements arranged in two different orientations are investigated. Simulated and measured results verify the effectiveness of the proposed technique, which constitutes the reduction in  $\rho$  for both isotropic and non-isotropic propagation environments along with port-isolation enhancement without reducing the fractional bandwidth (FBW) in all of the six tested cases. Further results indicate a wide FBW having a minimum of 8.5% and a maximum of 33%, while radiation patterns with no extra backward radiation are obtained.

**INDEX TERMS** Additive Manufacturing, Correlation Coefficient, Decoupling, MIMO Patch Antenna

## I. INTRODUCTION

The evolution in wireless communication demands increased spectrum allocation. Most of the current and upcoming multiple-input-multiple-output (MIMO) based wireless standards are wideband, *i.e.* LTE (2.2-3.8 GHz), IEEE 802.11a WLAN (5.1-5.8 GHz) and 5G sub-6 GHz mid band (3.7-3.98 GHz). MIMO is one such technology which uses multiple yet independent data streams between antenna elements at both transmitting and receiving ends, not only to enhance the spectral efficiency but also to improve the link reliabilities without increasing the bandwidth or power [1]. The major factor that limits the achievable benefits of MIMO systems, especially for closely arranged antenna elements, is the high channel spatial correlation and the low antenna port-isolation.

The isolation level among wireless communication channels formed in a MIMO system is quantified by the correlation coefficient  $\rho$ . It is a function of the complex 3D radiation patterns of the antenna elements as well as the propagation environment. Generally, an isotropic propagation environment of balanced polarizations is considered, thereby making  $\rho$  a function of only the complex radiation patterns of the antenna elements [2]. It is a reasonable assumption for denser urban cellular networks. However, for a base station (BS) or access point the angular spread of the waves is usually limited (*i.e.* BS consists of many non-directional antenna elements), which represents a non-isotropic scattering environment. Since hundreds of antenna elements are equipped compactly at the BS side in a

limited physical space,  $\rho$  and mutual coupling of the ports (*i.e.*  $S_{xy}$ ) becomes high as the spacing between antenna elements decreases. Moreover, in a non-isotropic environment,  $\rho$  further increases as the angular spread of the wireless channel decreases [3]. Thus, to ensure overall good performance of the MIMO system, the antenna design should induce low antenna port coupling and correlation among communication channels in both isotropic and non-isotropic multipath environments [4].

Due to computational complexities, a much simpler expression was developed in [5], which uses  $S$ -parameters based expression to evaluate  $\rho$  for lossless MIMO antennas. However, it has been shown in [6-7] that this expression leads to inaccurate results in most of the cases because not only all practical printed antennas are lossy but also this expression does not consider the orientation of the far-field pattern of antenna elements which actually connects the antenna spatial behavior to that of the wireless channels. It is also evident from the original formulation of  $\rho$  in [2] that the main factor for  $\rho$  evaluation is each antenna element's radiation pattern (and the actual propagation environment).

The value of  $\rho$  can be reduced by decorrelating either the magnitude, phase or polarization of the electric fields of the two or more radiating elements. In recent years, several works have been proposed on field decorrelation concept [3-4], [8-10]. The phase correcting elements (PCE) in [3] can effectively reduce the value of  $\rho$  by adjusting the near-field phase distributions of the MIMO antenna elements but the total efficiency remains low due to the high mutual coupling with and without the PCE. To mitigate this issue a planar metamaterial structure (PMS) and an array-antenna decoupling surface (ADS) are used to simultaneously achieve the decorrelation and decoupling of the MIMO antenna elements [4]. A phase-gradient partially reflective surface (PRS) is used above MIMO antennas in a Fabry-Perot cavity configuration to achieve field decorrelation by tilting the beams in opposite directions. However, the increase in mutual coupling between the patch-based MIMO antenna elements [8] due to the presence of the reflecting surface above them and the surface wave coupling, is a major drawback associated with this technique. In [9], a combination of three different narrow band PRS is used as superstrate for multiband performance enhancement of a MIMO antenna. Moreover, the narrow band feature of the PCE, PMS/ADS and PRS makes these types of methods less appealing for wideband applications.

Closely spaced antenna elements suffer from high mutual coupling values that cannot only reduce the radiation efficiency and signal-to-interference-noise ratio (SINR) of a propagation channel, but also results in spectral regrowth in some applications [11]. Subsequently, a variety of decoupling techniques has been reported in literature for coupled patch-based MIMO antenna elements, including defected ground structures (DGS) [12-14], meta-atoms structures [15-17] and parasitic based decoupling elements [18-21]. Each technique has its own drawback. For example, the use of the DGS in

patch-based antenna arrays affects the radiation features of the radiating elements, *i.e.*, not only the gain but also the front-to-back (FBR) is reduced [12-14]. The subwavelength structures of meta-atoms, including EBG / modified-SRR structures [15-16] and capacitively loaded loop meta-atoms superstrate [17] increase the geometrical complexities and limit their utilization for closely arranged MIMO patch array since such structures require large implementation space in-between the antenna elements. The use of parasitic elements above or in-between the patch radiating elements degrade the polarization purity [19] and considerably reduce the fractional bandwidth (FBW) of the decoupled patch antenna elements [20-21]. Moreover, most of the above decoupling techniques suffer from narrow impedance bandwidth response and are effective for only the fundamental resonant mode of the antenna (*i.e.*  $TM_{01}$  for a patch), which can limit their utilization for wideband applications [12-21].

To the best of the authors knowledge, not much attention has been given to achieve simultaneous field decorrelation and decoupling for wideband MIMO antenna elements because there has been a misconception that increasing the port-isolation guarantees  $\rho$  reduction. It has been shown that MIMO antenna ports decoupling alone does not always guarantee  $\rho$  reduction, especially in a realistic multipath environment [3]. Therefore, such decoupling solutions becomes unreliable in order to achieve enhanced MIMO performance especially in a realistic scenario.

In view of the above considerations, a wideband field decorrelation technique for coupled wideband MIMO antennas is still lacking, which can not only guarantee reduction in the values of  $\rho$  across the whole band for both isotropic and non-isotropic multipath environments but can also reduce mutual coupling without decreasing the FBW of each antenna element. This work presents a new technique for simultaneous reduction of the value of  $\rho$  and mutual coupling of wideband MIMO antenna elements by using a broadband graded index all-dielectric (GID) lens designed using transformation electromagnetics (TE). We introduced the concept of field decorrelation of a 2-element narrowband patches only in [22], wherein the mutual coupling reduction was insignificant. In this work, a broadband GID lens is designed to control the propagation direction of the electromagnetic (EM) wave and is fabricated using 3D printing. The lens reduces the radiation pattern spatial overlap when placed above wideband, multiband and ultra-wideband MIMO antenna elements, by tilting the beams in opposite directions. Besides, the port-isolation is also significantly improved by controlling the free space propagation constant by means of the latter GID lens, which in turn allows to suppress the surface wave propagation for antenna port decoupling. The attractive features of the proposed technique are summarized as:

1. Effective for patch-based MIMO antenna elements arranged in different positions or orientations.
2. Wideband performance enhancement is achieved when applied to a wideband patch-based MIMO antenna

- operating in two different modes as opposed to [3-4], [8].
3. Preservation of the radiation features and fractional bandwidth of the original MIMO antenna elements.
  4. Wider usability and intrinsic wideband phase matching at the interfaces for different antenna types working at different frequency bands. This feature is not being achieved by any previously reported work on field decorrelation and decoupling.
  5. Improvement of the isolation between adjacent elements.

The rest of the paper is organized as follows. Section II describes the GID lens design methodology. Section III presents the PLA-based GID lens, designed by using the guidelines detailed in Section II. Section IV presents the simulated and measured results of the considered examples, and Section V concludes the paper with a summary of the presented study.

## II. DESIGN METHODOLOGY

In a patch-based MIMO antenna, high spatial correlation caused by radiation pattern overlap, and high mutual coupling occurs due to existence of surface waves in the substrate [23]. The high spatial correlation can be reduced by tilting the individual antenna element beams in opposite directions. A graded index all-dielectric (GID) lens with a varying permittivity profile can be employed to achieve such a beam tilt for each antenna element. A systematic approach of TE is used here to evaluate the relation between the required beam tilt angle and the permittivity profile of the GID lens.

TE is a spatial transformation scheme which involves replacing the original space with a transformed space to control the wave-material interaction in a desired manner by defining the coordinate transformation based analytical mapping functions [24]. This technique is based on the form-invariance of Maxwell's equations under coordinate transformation. The material properties obtained by using this underlying principle, will mimic the distorted deformed space in the same manner as defined by spatial coordinate transformation functions and can perfectly recreate the same functionality of wave propagation as described in the original space by adjusting the variables of Maxwell's equations [25].

In the transformed space, the variation in all the tensor components of material parameters is quite complicated and generally requires anisotropic and dispersive materials for their realization. Meta-atoms are usually used to synthesize such material parameter distribution, but they suffer from narrow band frequency operation due to their resonant nature, and their magnetic response is accompanied by large absorption. An optimized design can be obtained by using quasi-conformal transformation electromagnetics (QCTE) mapping for which the requisite requirement of anisotropy along with magnetic response can be minimized. This design strategy allows the practical realization of TE devices from purely graded index all-dielectric (GID) materials that are non-

resonant as well as quasi-isotropic [26-27]. Such material properties imply broad operational bandwidth characteristics.

Here, we utilize QCTE mapping for the design of a broadband all-dielectric based beam steering symmetric lens which transforms the angle between an axis and wave vector. First, the desired pattern is defined by means of EM wave propagation in an air-filled virtual space. This pattern is then transformed to the physical space, which represents the transformed medium [28]. This medium achieves the similar function of EM wave propagation as defined in the virtual space, which will be demonstrated later. The calculated material properties of the transformed medium have a quasi-isotropic GID profile, with a slight in-plane anisotropy that can be ignored [29], in which only one component tensor of permittivity has spatial inhomogeneity. According to Fermat's principle of geometry of light, an inhomogeneous refractive index profile of the transformed medium allows to modify the trajectory of wave propagation to a desired direction. Thus, by associating the varying refractive index to transformed coordinate, the direction of wave trajectory can be controlled in the transformed medium. Hence, placing a symmetric GID lens above the MIMO patch elements will help reducing the radiation pattern spatial overlap by steering the beams in opposite directions.

However, as reported in previous works [22, 30], the drawback of TE based concept for field decorrelation is that the reduction in mutual coupling is insignificant in MIMO antennas, as the material parameters are not able to suppress the surface waves propagation in the antenna's substrate. With some minor adjustment in the inhomogeneous TE permittivity profile, the free space propagation constant can be further modified with the aim to completely suppress the surface waves propagation in the antenna substrate which results in significant port-isolation enhancement particularly in patch like MIMO antennas. This minor adjustment in the TE permittivity profile is based on the cut-off frequency formulations of transverse magnetic and transverse electric surface wave modes propagation inside a grounded dielectric slab waveguide, illustrated in Fig. 1, which has been well studied in [31]. Using this model, the cut-off frequency of different surface wave modes in the antenna substrate is given as [31]:

$$f_{CM} = \frac{mc}{2h\sqrt{\epsilon_1 - \epsilon_2\mu_2}}, \quad m = 0, 1, 2, 3, \dots \quad (1)$$

For the transverse magnetic mode, and as:

$$f_{CE} = \frac{(2n-1)c}{4h\sqrt{\epsilon_1 - \epsilon_2\mu_2}}, \quad n = 1, 2, 3, 4, \dots \quad (2)$$

for the transverse electric mode.  $\epsilon_1$  ( $\mu_1$ ) is the permittivity (permeability) of the substrate with thickness  $h$ ,  $\epsilon_2$  ( $\mu_2$ ) is the permittivity (permeability) of free space.

According to above equations, the cut-off frequency for each surface wave mode can be made infinite with  $\epsilon_1 = \epsilon_2\mu_2$ ,

which renders complete suppression of surface waves modes propagation in the antenna substrate. This specifies that by loading the patch MIMO antenna with a material whose effective  $\epsilon_2 \times \mu_2$  product equals  $\epsilon_1$  yields surface wave suppression. The required product value in our case will be achieved by loading the antenna elements either with a standard GID lens or a modified GID lens which also contains a homogenous dielectric slab having effective permittivity  $\epsilon_2 = \epsilon_1$  and permeability  $\mu_2 = 1$ . Thus, the proposed objective of field decorrelation and antenna port decoupling can be simultaneously achieved for such MIMO antennas by using a modified TE permittivity profile based symmetric GID beam steering lens.

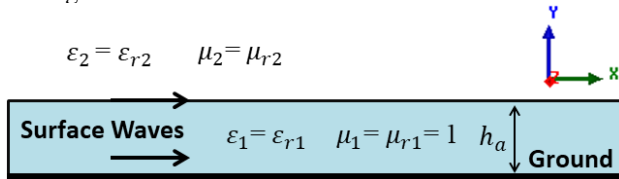


Fig. 1. Model of the grounded dielectric slab waveguide.

### III. STUDY OF FIELD DECORRELATED MIMO ANTENNAS

In this work, the far-field radiation patterns are obtained by exciting one element and terminating the other with 50  $\Omega$  matched load. The correctness of few MIMO antenna design examples is verified from the measured radiation patterns which are well consistent with the simulations. Also, due to the measurement conditions constraints, the value of  $\rho$  in all the examples considered in this work is evaluated using the simulated radiation patterns. The value of  $\rho$  of the MIMO antenna in an isotropic and non-isotropic propagation environment are evaluated in a post processing step using CST MWS simulation software.

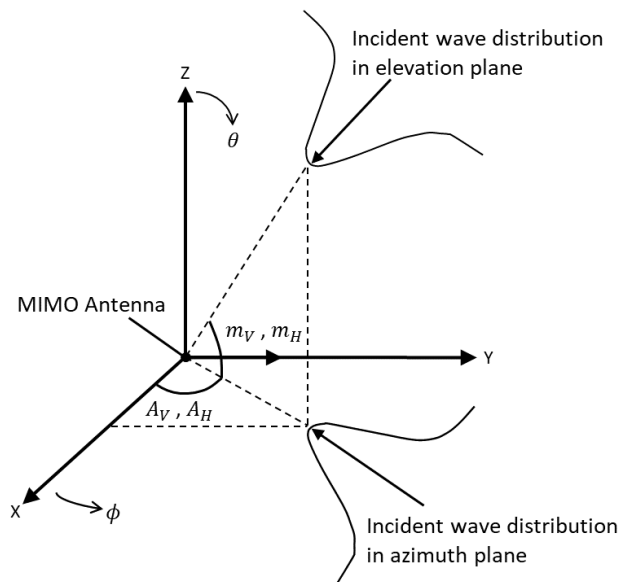


Fig. 2. Gaussian distribution model of incoming radio waves in a multipath propagation environment.

### A. CORRELATION COEFFICIENT OF MIMO ANTENNAS

The correlation coefficient ( $\rho$ ) evaluation is a crucial step to determine how much diversity (and capacity) a MIMO antenna design can provide in any propagation environment. It describes the statistical similarity between the radiation patterns of two arbitrary MIMO antenna elements. For an isotropic environment,  $\rho$  is evaluated using Equation (3), which considers the antenna far-field radiation patterns along with their polarizations and relative phase between the fields [3]:

$$\rho = \frac{|\iint_{4\pi} [\vec{F}_1(\theta, \phi) * \vec{F}_2(\theta, \phi)] d\Omega|}{\sqrt{\iint_{4\pi} |\vec{F}_1(\theta, \phi)|^2 d\Omega \iint_{4\pi} |\vec{F}_2(\theta, \phi)|^2 d\Omega}} \quad (3)$$

where  $\Omega$  is the solid angle,  $\vec{F}_i(\theta, \phi)$  ( $i = 1, 2$ ) is the complex 3D far-field radiation field of the  $i$ -th antenna, when only the  $i$ -th element is excited, and “\*” is the Hermitian product.

An isotropic scattering environment has a uniform incident wave distribution (*i.e.* waves arrive equally from all directions) and a cross-polarization ratio  $XPR = 1$ . However, a realistic multipath propagation environment is not isotropic, and the incident waves in such an environment have limited angular spread. Also, MIMO antenna correlation performance in a realistic environment is drastically different. The value of  $\rho$  is affected by both the antenna design and the propagation environment. Specifically, the spatial correlation at the MIMO antenna increases due to non-uniform angular power spectrum (APS) distribution or limited angular spread of the incident waves [32]. Therefore, a more general expression for  $\rho$  evaluation that considers the actual environment effect can be expressed as [3]:

$$\rho = \frac{|\int_{\Omega} B_{ij}(\Omega) d\Omega|}{\sqrt{\int_{\Omega} B_{ii}(\Omega) d\Omega \cdot \int_{\Omega} B_{jj}(\Omega) d\Omega}} \quad (4)$$

with,

$$B_{ij}(\Omega) = XPR \cdot F_{\theta i}(\Omega) F_{\theta j}^*(\Omega) P_{\theta}(\Omega) + F_{\phi i}(\Omega) F_{\phi j}^*(\Omega) P_{\phi}(\Omega) \quad (5)$$

where  $XPR$  is the cross-polarization ratio between the vertical polarized (VP) and horizontal polarized (HP) incident power densities,  $F_{\phi i}$  and  $F_{\theta i}$  represent the  $\phi$  (azimuth) and  $\theta$  (elevation) components of  $\vec{F}_i$ ;  $P_{\phi}(\Omega)$  and  $P_{\theta}(\Omega)$  are the APS distributions of the  $\phi$  and  $\theta$  components of incident waves in the propagation environment, respectively. The multipath propagation environment characteristics are defined by the APS distribution of the incident waves at the MIMO antenna system. A few models of the APS distribution like Gaussian, Laplacian and Elliptical, along with their typical parameter values for different propagation environment scenarios have been reported in [33]. The direction and the angular spread of the incident wave can be controlled using these models. In this work, the Gaussian APS distribution model in both

elevation and azimuth planes is considered for both VP and HP waves [34], as shown in Fig. 2. The expressions for the Gaussian APS distribution are given as [34]:

$$P_{\theta}(\theta, \phi) = A_{\theta} \cdot \exp \left[ -\frac{\left\{ \theta - \left[ \left( \frac{\pi}{2} \right) - m_v \right] \right\}^2}{2\sigma_v^2} \right] \cdot \exp \left[ -\frac{(\phi - A_v)^2}{2\delta_v^2} \right], (0 \leq \theta \leq \pi, 0 \leq \phi \leq \pi) \quad (6)$$

$$P_{\phi}(\theta, \phi) = A_{\theta} \cdot \exp \left[ -\frac{\left\{ \theta - \left[ \left( \frac{\pi}{2} \right) - m_H \right] \right\}^2}{2\sigma_H^2} \right] \cdot \exp \left[ -\frac{(\phi - A_H)^2}{2\delta_H^2} \right], (0 \leq \theta \leq \pi, 0 \leq \phi \leq \pi) \quad (7)$$

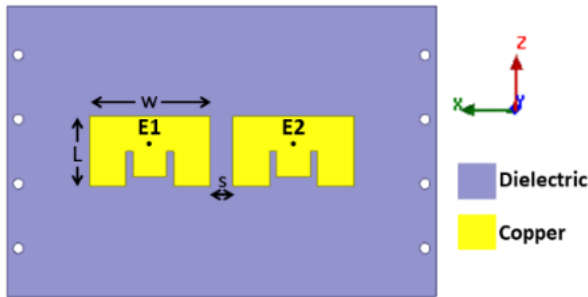


Fig. 3. H-plane coupled 2-element E-patch MIMO antenna.

where  $m_v$  and  $m_H$  are the mean elevation angles of the VP and HP wave distributions observed from the horizontal direction respectively;  $\sigma_v$  and  $\sigma_H$  are the standard deviations of the VP and HP wave distributions respectively;  $A_v$  and  $A_H$  are the mean azimuth angles of the VP and HP wave distributions respectively; and  $\delta_v$  and  $\delta_H$  are the standard deviations of the VP and HP wave distributions respectively. In Equations (6) and (7) the standard deviation value defines the angular spread of the incident wave. Here,  $\rho$  of the proposed MIMO antenna is evaluated by setting  $XPR = 5$  dB,  $m_v = m_H = A_v = A_H = 0^\circ$  and  $\sigma_v = \sigma_H = \delta_v = \delta_H = 30^\circ$ . These values are reasonable assumptions for an access point application, where all the users mean angle remain close to the broadside direction of the MIMO antenna array.

### B. H-PLANE COUPLED 2-ELEMENTS WIDEBAND MIMO ANTENNA

To investigate the wideband field decorrelation and port decoupling concept using the proposed GID lens, H-plane coupled antenna elements are considered. They consist of a 2-element E-shaped patches with edge separation of 10 mm ( $0.1\lambda$ ), as shown in Fig. 3, operating around 3 GHz and designed on a 3.2 mm thick FR4 substrate ( $\epsilon_{r1} = 4.4$ ) with lateral dimensions  $133 \times 90$  mm<sup>2</sup>. The dimensions ( $L / W$ ) of each patch are 21.7 mm / 37.5 mm and are excited using coaxial offset feeds.

The simulated scattering parameters of this antenna configuration are shown in Fig. 4(a). It can be seen that a wide -10 dB fractional bandwidth (FBW) from 2.903 to 3.216 GHz (10.2%) is obtained due to two resonant frequencies at 3 GHz

( $TM_{01}$ ) and 3.1 GHz ( $TM_{02}$ ), respectively. The lowest isolation level between the two antenna ports in the -10 dB FBW is 14 dB. The simulated 2D far-field normalized radiation patterns of this configuration in the  $xoy$ -plane are shown in Fig. 4(b). It can be seen that each antenna element has a typical radiation pattern of a patch antenna, which is slightly tilted due to existence of surface waves and adjacent metallic element in close proximity. At 3 GHz, the boresight direction of beam maxima of the antenna elements E1 and E2 without the lens are at  $20^\circ$  and  $-20^\circ$  respectively, (*i.e.* both the beams have opposite crossing directions). As shown in Fig. 4(c), this cross tilting of beam maxima's results in high  $\rho$  for both isotropic and non-isotropic propagation environments, due to high radiation pattern spatial overlap. The low antenna port-isolation and high  $\rho$  will degrade the achievable channel capacity of the MIMO system [3].

### C. GRADED INDEX ALL-DIELECTRIC (GID) LENS

Field decorrelation can be achieved by designing the antenna elements in such a way that their 3D radiation patterns are as orthogonal to each other as possible, *i.e.* their beams are tilted in opposite directions resulting in a minimum radiation patterns spatial overlap. A steering angle greater than  $\mp 15^\circ$  for each beam from broadside, is considered sufficient for decorrelating the fields [35]. Thus, we want to steer the antenna element beams by greater than  $\mp 15^\circ$  from the proposed GID lens.

The symmetric GID lens design for 2-element beam tilting is based on the methodology discussed in Section II and the theoretical model detailed in [28]. To steer the antenna element beams by greater than  $\mp 15^\circ$  from a TE based quasi-isotropic all-dielectric lens, a steering angle of  $\mp 45^\circ$  need to be imposed because the ideal calculated TE based lens will indeed present such  $\mp 45^\circ$  steering performance, but with anisotropic material parameters tensor. To fulfill the all-dielectric requirements, the anisotropy in the material parameters tensor is ignored, which results in a drop of the steering angle to about  $\mp 28^\circ$ , as will be shown later. Therefore, the EM wave propagation is first described in an air-filled virtual space to provide a beam tilt of  $\mp 45^\circ$  as shown in Fig. 5(a). The angle between the  $y$ -axis and wave vector is set to  $\mp 45^\circ$ . QCTE mapping is then applied to find a transformed medium with a varying permittivity in the physical space, which creates the same degree of beam tilt as described in the virtual space. The Laplace's equation is used to determine the transformation matrix by solving it using the COMSOL Multiphysics partial differential equation (PDE) solver subject to predetermined Dirichlet and Neumann sliding boundary conditions. The obtained field profile due to the transformed medium is shown in Fig. 5(b), which indicates same beam tilt angle of  $\mp 45^\circ$  is attained as defined in virtual space. The QCTE mapping between the virtual and physical space is illustrated in Fig. 5(c). Moreover, the size of the transformed medium must be big enough to cover both antennas otherwise smaller beam deflection will be obtained. Thus, each transformed medium area is assumed to be  $59.5 \times 35$  mm<sup>2</sup>.

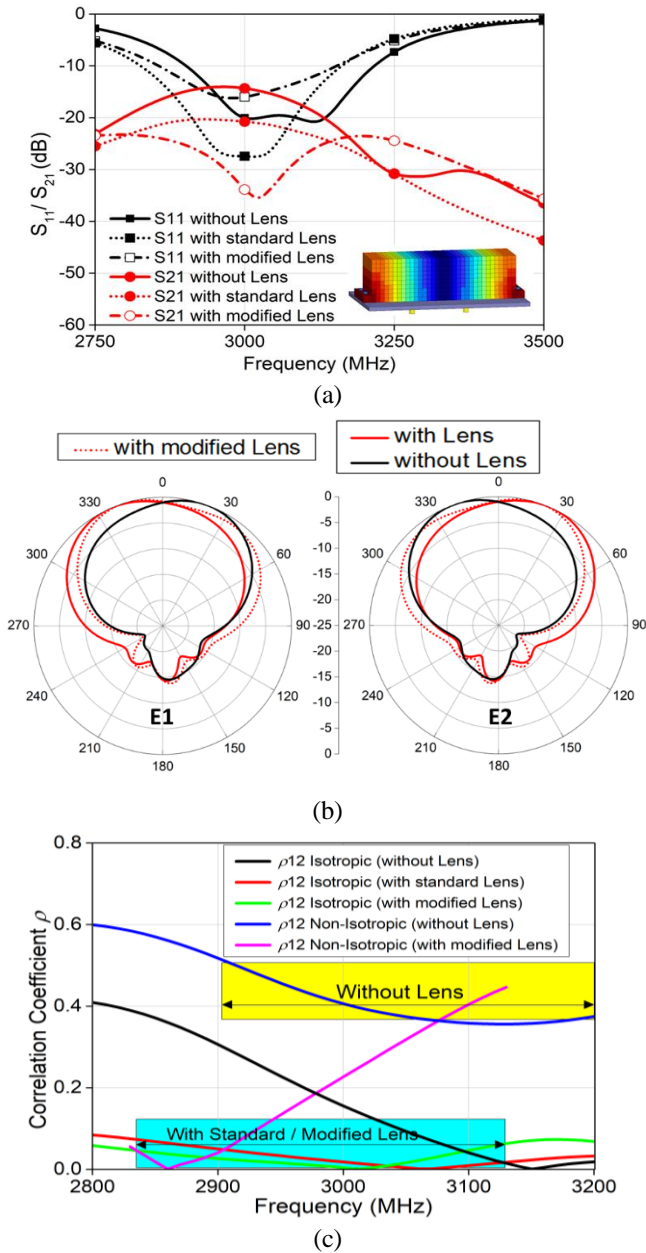


Fig. 4. Simulated results of 2-elements MIMO antenna with and without lens. (a)  $S$ -parameters. (b) Normalized radiation pattern E1 and E2 in the  $xoy$ -plane at 3 GHz. (c) Correlation coefficient.

The transformed medium profile obtained for the beam tilting presents anisotropic material parameters which are difficult to physically realize. The deformation in the physical space due to space transformation is shown in Fig. 5(c). The physical space conformal module, a geometric quantity determined by the structure of the space and containing the complete invariants of the structure, is greater than 1, as compared to the virtual space which is 1, resulting in anisotropy in the transformed medium. However, we propose to ignore the anisotropy in the material parameter tensor for a possible experimental demonstration of the symmetric GID lens beam steering functionality using an isotropic graded

index all-dielectric material. Since the conformal module is larger than 1, such parametric reduction in tensor components weakens the beam steering functionality, which is reduced to  $28^\circ$  as shown in Fig. 5(d), which is sufficient for our beam tilting. As the transformed medium permittivity profile has a continuous variation, a discretization procedure is then applied according to which the inhomogeneous permittivity profile of the proposed lens is varied in discrete steps between 1 and 2.8, as shown in Fig. 5(e), which then represents the transformed medium. The host dielectric polylactic acid (PLA) material available in our 3D printing facility has a relative permittivity of 2.65, the permittivity values in the discrete profile higher than 2.65 are supposed to be equal to the relative permittivity of the PLA. The obtained structure of the lens consists of 340 ( $34 \times 10$ ) unit cells with an elementary cell dimension of  $3.5 \times 3.5 \times 40 \text{ mm}^3$  each.

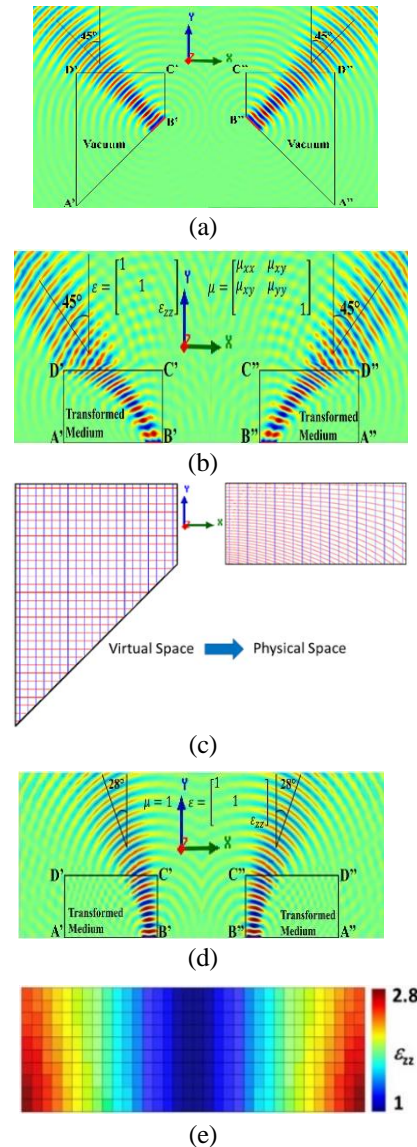


Fig. 5. Space mapping illustration. (a) Air-filled initial virtual space. (b) Calculated transformed ideal anisotropic lens. (c) QCTE mapping from virtual space to physical space. (d) Calculated simplified quasi-isotropic lens. (e) Permittivity ( $\epsilon_{zz}$ ) profile of simplified quasi-isotropic lens.

The discrete symmetric GID lens is placed symmetrically above the 2-element E-shaped patch MIMO antenna, as shown in the inset of Fig. 4(a), such that at the centre the relative permittivity is 1 and its value increases in steps as we move on either side of the  $x$ -axis with highest value of 2.65 at the edges. To keep the branch power ratio close to 1, the lens is placed symmetrically above the antenna, an attribute which is recommended for MIMO antennas [36]. The discrete symmetric GID lens can decorrelate the fields as the radiation patterns of antenna element E1 / E2 are tilted in opposite directions (*i.e.* no cross tilting of the beams) with beam maximas are tilted by around  $-25^\circ / 25^\circ$  as shown in Fig. 4(b). Besides, it can be seen in Fig. 4(a) that the lens loaded antenna elements demonstrate almost the same wide simulated FBW of 11.2% (2.826-3.162 GHz) with reduced  $\rho$  value for both propagation environments while the port-isolation enhancement is only 6.7 dB, which is considered insignificant in many applications. For example, in communication system several power amplifiers nonlinearity together with strong port coupling causes spectral regrowth, resulting in adjacent channel interference or crosstalk [11]. The spectral regrowth can be reduced by improving the port-isolation  $S_{21}$  level even below -28 dB or more [37]. The port-isolation enhancement with the GID lens is primarily caused by tilting of the beams without creating a cavity, as there are insignificant reflections from the lens as compared to PRS-based Fabry-Perot cavity beam tilting method described in [8], and minimal suppression of the surface waves propagation in the antenna substrate.

To further improve the port-isolation by means of surface waves propagation suppression, a slight adjustment in the TE permittivity profile of the lens can be made either by adding a homogenous dielectric slab in the center of that discrete profile at a certain offset distance  $m$  from the substrate, as shown in Fig. 6, or by bringing the higher values of the TE permittivity profile distribution above the patch element using the reduced unit cell dimensions.

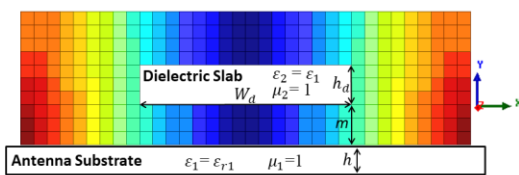


Fig. 6. Schematic of the modified GID lens loaded E-patch MIMO antenna elements.

In the first case, the offset distance  $m$  is determined based on the surface waves propagation inside the dielectric substrate. According to [31], surface waves are categorized by a field that decays exponentially away from an interface between two different media, with most of the fields restricted inside or near the dielectric interface. Since strong electric (fringing near) field distribution is present above the patch antenna which decreases away from the patch, the major contributing factor for high port-isolation is the surface waves which are present around the dielectric interface. In order to effectively control and suppress the surface waves propagation for port-isolation enhancement, without affecting the steering

performance of the GID lens, the initial offset distance  $m$  of the dielectric slab from the substrate assumed to be less than  $0.35\lambda$ . As detailed in Section II, the added dielectric slab should have effective permittivity  $\epsilon_2 = \epsilon_1 = \epsilon_{r1} = 4.4$  and permeability  $\mu_2 = 1$  in order to achieve the required product  $\epsilon_2 \times \mu_2 = 4.4 = \epsilon_1$  value for complete suppression of surface wave propagation inside the antenna substrate which results in more than 23 dB port-isolation enhancement at 3 GHz, as shown in Fig. 4(a), with almost same wide FBW of 10% (2.835-3.129 GHz). The slight shift in resonant frequency, when antenna elements are loaded with a lens, is primarily due to the change in the effective permittivity of the patch antenna.

Fig. 4(b) shows that the beam tilt angle for each element is reduced to  $\mp 18^\circ$  in the modified case which is still greater than the  $\mp 15^\circ$  optimal beam tilt angle requirement set for field decorrelation. Please note that this is the proper non-crossing tilt. The decrease in the beam tilt angle is due to the placement of the dielectric slab in the TE permittivity profile of the lens which has slightly modified the refractive index profile of the GID lens. Although  $\rho$  is reduced with the modified GID lens also, its value is almost the same as compared to the standard GID lens, as shown in Fig. 4(c). This shows that further increase in port-isolation cannot guarantee more  $\rho$  reduction for both isotropic and non-isotropic propagation environments. However, with the standard GID lens, the reduction in  $S_{21}$  value is insufficient and, further reduction with the modified GID lens is still necessary to obtain good radiation efficiency. It also improves the SINR of a propagation channel and in certain applications reduces the spectral regrowth. The initial dimensions and the offset distance  $m$  of the dielectric slab in the modified lens profile are optimized ( $W_d = 56$  mm,  $H_d = 10.5$  mm,  $m = 10.5$  mm) to get the maximum port-isolation enhancement within the FBW of each antenna element.

It is important to note that the maximum value in the overall permittivity profile of the modified GID lens is 4.4, when antenna elements are designed on FR4 substrate ( $\epsilon_r = 4.4$ ), which cannot be accessed from a PLA filament with a dielectric constant of 2.65, but the gradient lower than 2.65 can still be realized from the same filament. Hence, in this work the inhomogeneous discrete permittivity profile of the modified symmetric GID lens is designed from single PLA filament available in our printing facility, whereas the required permittivity of the homogeneous dielectric slab can be realized either from a single slab of required thickness or by multi layers stacking of the substrate without copper cladding. The number of layers required will be based on the thickness of the dielectric slab. Since the required permittivity of the dielectric slab is 4.4 therefore a 1.6 mm thick FR4 substrate with same optimized lateral dimensions is used in six multi layers stacking configuration to achieve the desired thickness of the dielectric slab which is 9.6 mm. The fabrication complexity can be reduced if a dual extruder 3D printer is used, such that the same lens sample can be easily printed in a single step by using two different PLA filaments of desired permittivity.

The discrete permittivity profile gradient lower than 2.65 of the GID lens is realized from non-resonant dielectric cube like cells with air holes of different dimensions, as shown in Fig. 7(a), with the objective to use the lens over a broad frequency range. The permittivity value of each unit cell should be homogeneous across the cell. By using effective medium theory, this can be accomplished by using a very small sized unit cell as compared to the operating wavelength. The required effective permittivity of the unit cell consists of two materials, namely air and dielectric, can be designed by varying the thickness ' $t$ ' and radius ' $r$ ' of the dielectric part of the unit cell while keeping the periodicity along  $z$ -axis  $P_z = 5$  mm [26]. Parameter retrieval method is used to numerically characterize the effective permittivity of the dielectric unit cells [38]. The standard and modified GID lens without dielectric slab is fabricated using 3D printing technology [39]. A plastic PLA filament, having a dielectric constant of 2.65 and loss tangent of 0.0062 at 3 GHz, is used for the printing process.

The geometry of the designed and fabricated PLA-based lens loaded 2-element E-shaped patch MIMO antenna is shown in Fig. 7(b). The dimensions of the modified GID lens are  $119 \times 35 \times 40$  mm<sup>3</sup> which can easily cover both antenna elements. Two 1.6 mm thick FR4 boards are stacked to achieve the desired 3.2 mm thickness of the antenna substrate. In order to mount the GID lens above the antenna elements two support edges of width 7 mm each with four M3 holes are added.

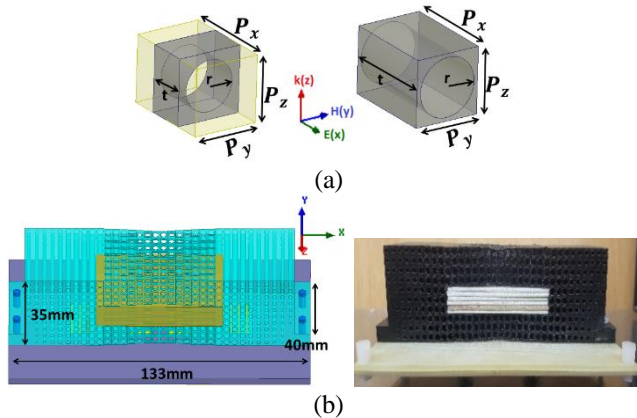


Fig. 7. (a) Dielectric unit cell for effective permittivity of 1.25 and 1.63, where  $P_x = 5$  mm,  $P_y = P_z = 3.5$  mm. (b) Geometry of the lens loaded 2-element H-plane decoupled MIMO antenna.

In the second case, the same standard GID lens of Fig. 5(e) can also further reduce the  $S_{21}$ , without modifying the permittivity profile distribution which ranges from 1 to 2.65 (*i.e.* without the homogeneous dielectric slab), by reducing the unit cell size of the standard GID lens to  $P_y = P_z = 3$  mm while assuming the same periodicity of 5 mm as shown in inset of Fig. 8(a). This size reduction brings the higher values of the permittivity profile distribution above the patch elements which generally helps to achieve the required product value for complete suppression of surface wave propagation. In this

case the complete suppression of surface waves is not possible because the maximum value in the permittivity profile is 2.65 and the required product value of  $\epsilon_2 \times \mu_2 = 4.4 = \epsilon_1$  cannot be achieved. However, more than 9.2 dB port-isolation enhancement is still achieved in this case at 3 GHz due to the slight surface waves suppression. The beam tilt angle is  $\mp 25^\circ$  with a low value of the  $\rho$  for both isotropic and non-isotropic propagation environments. In this case the edge to edge spacing between the antenna elements is reduced to  $0.05\lambda$  in order to get higher value of  $S_{21}$  and  $\rho$ . Although the port-isolation enhancement in the second case is not as large as compared to the first case but the beam tilt angle in the latter case remains preserved to  $\mp 25^\circ$ .

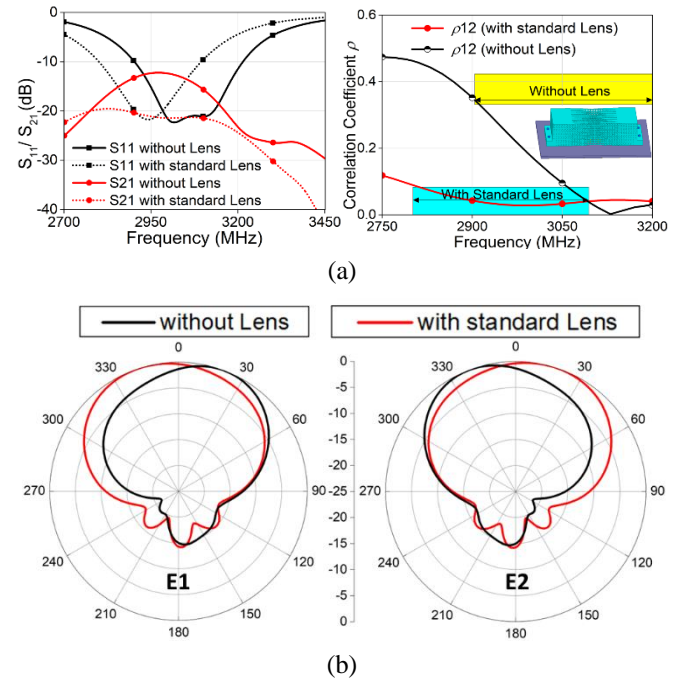


Fig. 8. Simulated results of 2-elements MIMO antenna with and without reduced unit cell size based PLA standard lens. (a)  $S$ -parameters and Correlation Coefficient. (b) Normalized radiation pattern E1 and E2 in the  $xoy$ -plane at 3 GHz.

#### D. DESIGN GUIDELINES

To ensure that the proposed method works efficiently for wideband MIMO antennas, it is essential to provide the design guidelines for GID lens, which are as follows:

1. To achieve the preferred beam steering functionality, the GID lens size must be big enough to cover both antenna elements. But there exists a trade-off between the desired bandwidth and the lens size for which a homogeneous transformed medium can be designed in any frequency range according to effective medium theory. Since the wavelength is large at the lower limit of the frequency range, this leads to larger lens size as compared to the upper frequency limit where size is restricted by the small wavelength. Therefore, at high frequencies, the unit cells must be engineered with respect to the wavelength so as to be consistent with the effective medium theory. Moreover, the height of the

lens is assumed to be equal to  $0.35\lambda$  since patch antennas have strong electric field distribution within this region.

- To obtain high port isolation in the whole band of interest two strategies can be employed. In the first option, initially set the permittivity  $\epsilon_2$  of the dielectric slab to be equal to the relative permittivity  $\epsilon_r$  of the antenna substrate with initial dimensions comparable to cover both antenna elements, and then optimize the slab lateral dimensions ( $W_d/h_d$ ) and offset distance  $m$ . In the second option, reduce the unit cell size of the standard GID lens. This reduction results in higher values of the permittivity profile distribution above the antenna elements which either helps to completely or slightly achieve the required product  $\epsilon_2 \times \mu_2 = \epsilon_1$  value for complete suppression of surface wave propagation.

A parametric study has been carried out in Fig. 9, to show the effects on antenna port-isolation firstly by using different permittivity  $\epsilon_2$  at fixed value of  $m$  and secondly by using different offset distance  $m$  of the dielectric slab at fixed value of  $\epsilon_2$ . It can be seen in Fig. 9(a) that more than 25 dB port-isolation enhancement is achieved at the resonance frequency with  $S_{21} \leq -20$  dB in the whole band when  $\epsilon_2 \geq 4.4$  but the FBW reduces considerably for  $\epsilon_2 > 4.4$  which is not desirable. On the other hand, it can be observed in Fig. 9(b) that after adopting the dielectric slab with permittivity  $\epsilon_2 = 4.4$ , the isolation frequency is sensitive to  $m$  and it decreases when the value of  $m$  is increased. Besides, the matching conditions nearly remain the same except for  $m = 0$  mm. At 3 GHz, the maximum port-isolation enhancement with the modified GID lens is achieved when  $m = 10.5$  mm, where it is improved from 14 dB to 40 dB.

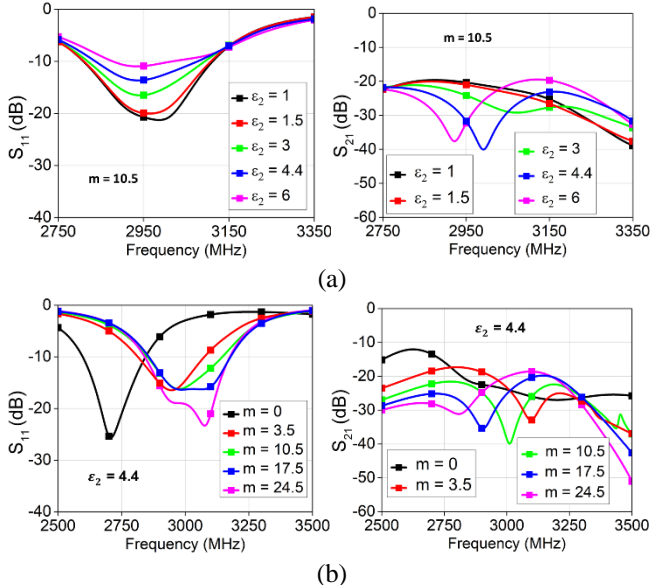


Fig. 9. Simulated  $S$ -parameters of GID lens loaded H-plane coupled 2-element E-patch MIMO antenna. (a) with different values of  $m$ . (b) with different  $\epsilon_2$  of dielectric slab.

## IV. RESULTS AND DISCUSSIONS

### A. H-PLANE COUPLED 2-ELEMENTS WIDEBAND MIMO ANTENNA

To verify the performance of the H-plane coupled 2-element MIMO antenna, the  $S$ -parameters are measured with and without the PLA-based modified GID lens. A good agreement between the simulated and measured results is obtained, as can be observed from Fig. 4(a) and Fig. 10(a), respectively. With (without) the lens, a wide -10 dB measured FBW of 8.5% from 2.933-3.193 GHz (10.5% from 3.030 to 3.366 GHz) is obtained. In addition, more than 25 dB port-isolation enhancement is achieved with the lens at the resonance frequency of 3.035 GHz when compared to the antenna alone, as shown in Fig. 10(a). The minor reduction in resonant frequency and FBW is primarily due to the non-uniformity in the relative permittivity of the FR4 substrate and the presence of the small air gap formed between the two FR4 layers due to fabrication limitations [40]. However, the agreement between simulated and measured FBW values is still satisfactory.

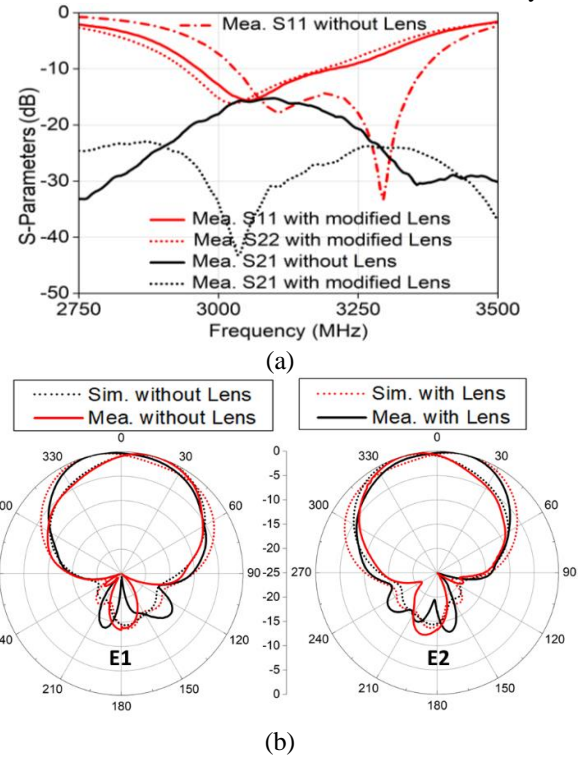


Fig. 10. Simulated and measured results of 2-element H-plane coupled MIMO antenna with and without lens. (a)  $S$ -parameters. (b) Normalized radiation pattern E1 and E2 in the  $xoy$ -plane.

The measured 2D normalized radiation patterns of each antenna element with and without the lens in the  $xoy$ -plane are shown in Fig. 10(b), which show good agreement with the simulation results. At the resonant frequency, the measured beam maxima of antenna elements E1 / E2 without the lens are slightly tilted to  $20^\circ$  /  $-20^\circ$  (crossed or opposite to the desired directions) and with the lens the measured beam maxima are oppositely tilted in the desired directions to  $-17^\circ$  /

17°, respectively, thereby decreasing the 3D radiation patterns spatial overlap. Besides measurement errors, the small variation in beam tilt angle is due to fabrication tolerances of the 3D printer which cause changes in permittivity profile. The gain and efficiency of each antenna element with (without) the modified GID lens within the desired FBW is 4.5-5.49 dBi (3.41-5.37 dBi) and 59.8%-65.4% (51.8%-62.4%), respectively, which indicate an enhancement in the presence of the lens. The efficiency improvement can be credited to the coupling reduction between the two antenna ports. Moreover, the presence of the lens has quasi no influence on the FBR.

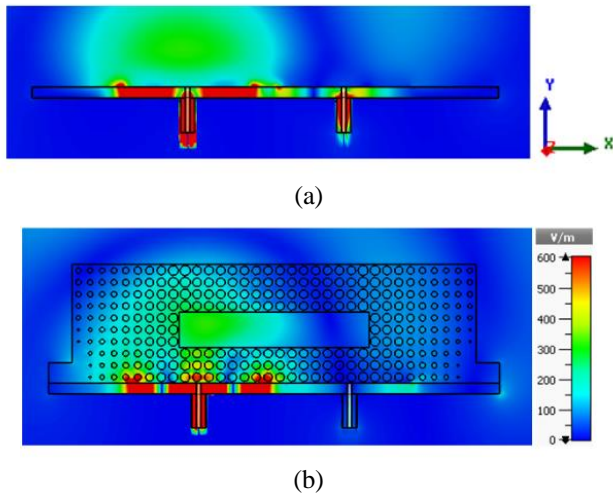


Fig. 11. E-field distribution of 2-element H-plane coupled MIMO antenna. (a) Without lens. (b) With lens.

The calculated  $\rho$  of the proposed MIMO antennas in their respective FBWs are plotted in Fig. 4(c). It is evident from Fig. 4(c) that for both isotropic and non-isotropic environments the  $\rho$  of the MIMO antenna alone presents higher values than when the proposed GID lens is placed above the antenna elements, *i.e.* with the lens  $\rho$  is reduced from around 0.301 to 0.025 for isotropic environment while for non-isotropic environment it reduces from 0.505 to 0.047 at 2.901 GHz (except at the higher end of the frequency band). This shows that the field decorrelation is significantly improved by tilting the 3D radiation patterns of MIMO antenna elements, enabling to achieve good diversity and multiplexing performances.

The electric field distribution of the 2-element E-shaped patch MIMO antenna with and without the GID lens at 3 GHz has been calculated when E1 is excited and plotted on the  $xoy$ -plane, as shown in Fig. 11, to further demonstrate the port-decoupling mechanism. In an unloaded case, strong electric field strength is present around element E2 when element E1 is excited as shown in Fig. 11(a), thus causing a high level of mutual coupling between the two antenna ports. It can be seen in Fig. 11(b) that after using the GID lens, the coupled electric field strength is drastically reduced that leads to high port-isolation. This reduction in coupling with the lens is due to complete suppression of surface wave propagation in the antenna substrate.

## B. E-PLANE COUPLED 2-ELEMENTS AND 6-ELEMENTS WIDEBAND MIMO ANTENNA

To further validate the generality of the proposed concept, now an E-plane coupled antenna element configuration operating around 3 GHz on a 3.2 mm thick FR4 substrate is considered, wherein the same two E-shaped patches are arranged in vertical directions with edge separation of 10 mm ( $0.1\lambda$ ), as shown in Fig. 12(a). Both the simulated and measured  $S$ -parameters of this configuration are shown in Fig. 13(a). A wide -10 dB measured (simulated) FBW of 10.8% from 2.950-3.288 GHz (10.2% from 2.893 to 3.205 GHz) is obtained with a minimum port-isolation level of 12 dB within the FBW. In order to improve the port-isolation by means of surface wave suppression within the desired frequency band, the offset distance  $m$  and the initial dimensions ( $W_d/h_d$ ) of the dielectric slab in the TE permittivity profile of the GID lens, as shown in inset of Fig. 13(a), are optimized as per the design guidelines provided in Section III-C. The designed and fabricated prototype of the PLA-based modified GID lens loaded MIMO antenna is shown in Fig. 12(c). The required product  $\epsilon_2 \times \mu_2 = 4.4 = \epsilon_1$  value is realized by using a FR4 dielectric slab having permittivity  $\epsilon_2 = \epsilon_1 = \epsilon_r = 4.4$  and permeability  $\mu_2 = 1$ . In this case, the optimized initial dimensions and the offset distance  $m$  of the dielectric slab are ( $W_d = 63$  mm,  $H_d = 10.5$  mm,  $m = 24.5$  mm). With the lens, more than 30 dB measured port-isolation enhancement is achieved at 3.16 GHz, as shown in Fig. 13(a), with measured (simulated) FBW of 10.2% from 2.945-3.260 GHz (9.7% from 2.890-3.185 GHz).

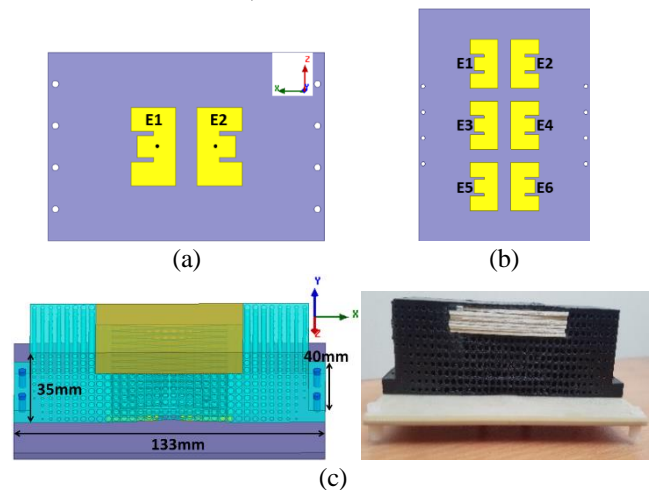


Fig. 12. (a) E-plane coupled 2-element E-patch MIMO antenna. (b) E-plane coupled 6-element E-patch MIMO antenna. (c) Geometry of the GID lens loaded 2-element MIMO antenna.

Fig. 13(b) shows the measured and simulated 2D normalized radiation patterns of both antenna elements in the  $xoy$ -plane before and after using the modified GID lens. It can be seen that a good agreement between simulated and measured results is obtained. At 3.175 GHz, the measured beam maxima's of E1 / E2 without the lens are slightly tilted to  $\pm 25^\circ$ , whereas the tilt in measured beam maxima's after

using the proposed lens remains the same, *i.e.*  $\mp 25^\circ$ . Without the lens the beam maxima's are tilted due to strong antenna port coupling. It is important to preserve the beam maxima's tilt angle with the lens otherwise if only the decoupling scheme is used than the beam maxima's turn back to the boresight  $+y$ -direction [20-21], which subsequently increases the  $\rho$  in realistic environment due to large 3D radiation pattern spatial overlap. The gain and efficiency of each antenna element with (without) the lens within the desired FBW is 4.2-5.4 dBi (3.3-5.1 dBi) and 48%-59.6% (46.6%-58.7%), respectively, which indicates a gain enhancement in the presence of the lens.

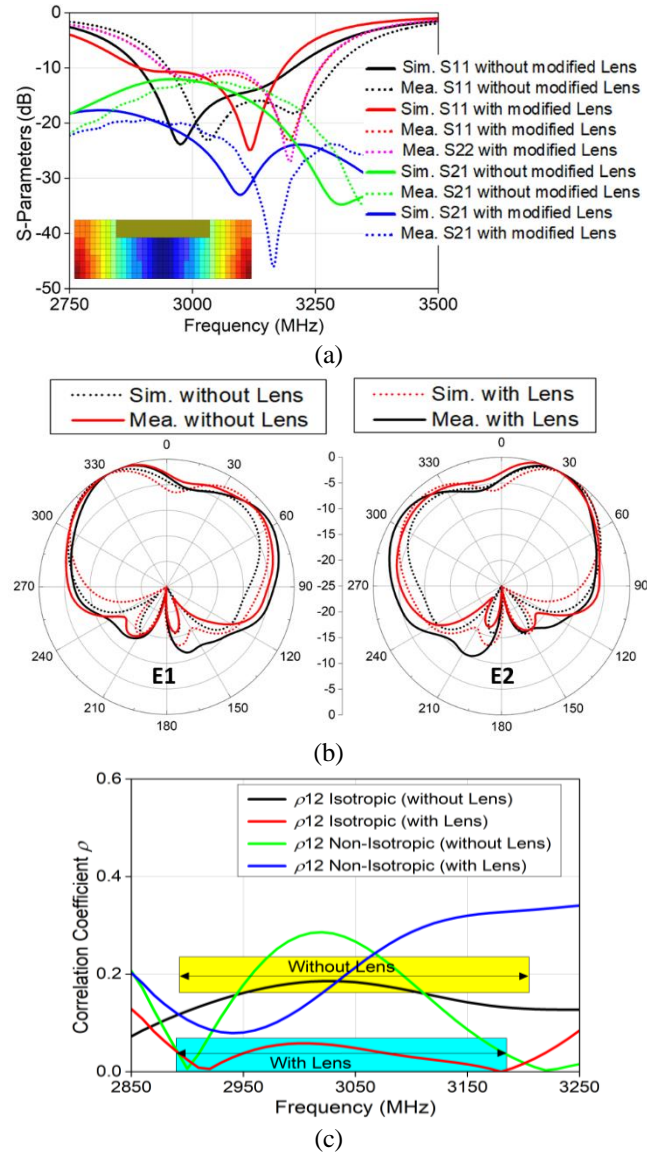


Fig. 13. Simulated and measured results of 2-elements E-plane coupled MIMO antenna with and without lens. (a) S-parameters. (b) Normalized radiation pattern E1 and E2 in the  $xy$ -plane. (c) Correlation coefficient.

Fig. 13(c) shows the plots of the calculated  $\rho$  of the proposed MIMO antennas in their respective FBW. Similarly, it is evident from the figure that the  $\rho$  of the MIMO antenna alone presents higher values when compared to antenna

elements with modified GID lens in case of isotropic environment, *i.e.* with the lens  $\rho$  remains less than 0.054 in the entire FBW. However, in non-isotropic environment the  $\rho$  reduction is mostly achieved in the lower half of the frequency band. This slight increase in  $\rho$  at the higher half of the frequency band is due to the non-uniform APS distribution [32]. Also, it is worthwhile to mention that the radiation patterns of antenna elements without the lens are already tilted in opposite direction, which will lead to lower values of  $\rho$  in isotropic environment, as radiation patterns spatial overlap is relatively small, when compared to  $\rho$  of H-plane coupled MIMO antenna elements. After using the lens, the  $\rho$  is reduced as the radiation pattern spatial overlap is further reduced due to improvement in gain.

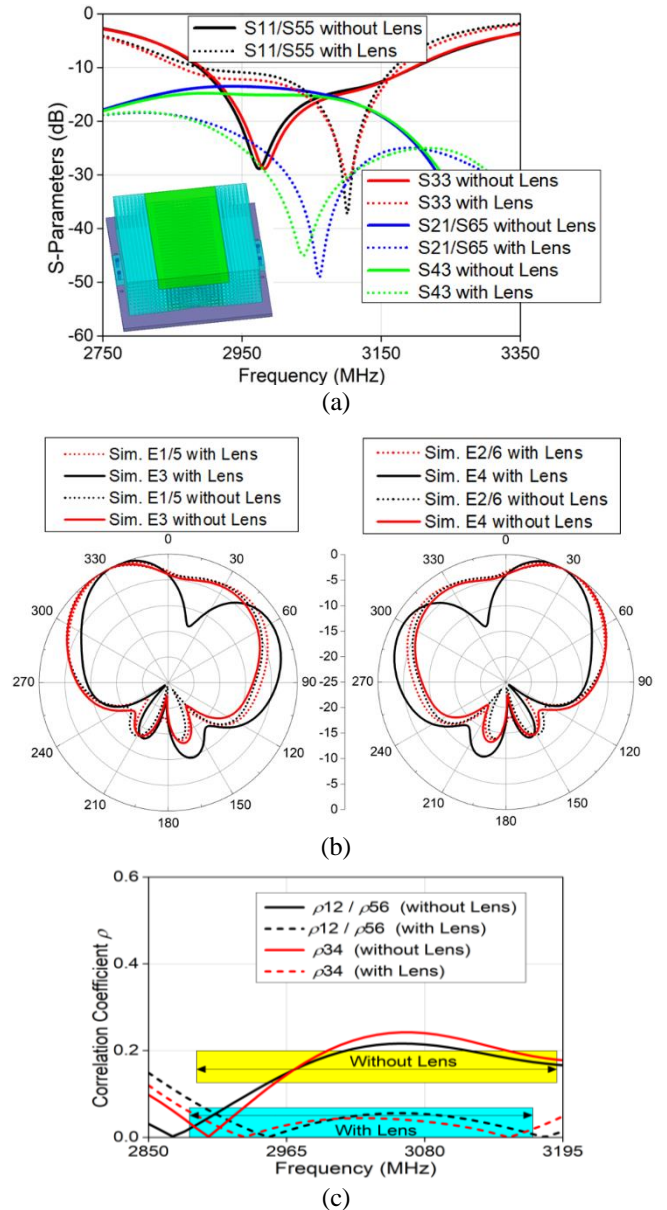


Fig. 14. Simulated results of 6-element MIMO antenna with and without lens. (a) S-parameters. (b) Normalized radiation pattern E1/ E3/ E5 and E2/ E4/ E6 in the  $xy$ -plane. (c) Correlation coefficient.

Moreover, the proposed GID lens utilization can be extended for field decorrelation and decoupling of E-plane coupled MIMO antennas having more than two elements, without modifying the lens permittivity profile. To demonstrate this feature, an E-plane coupled MIMO antenna with six elements is considered, as shown in Fig. 12(b), with edge separation of 10 mm ( $0.1\lambda$ ) at 3 GHz and lateral dimensions  $133 \times 180 \text{ mm}^2$ . The complete geometry of the modified GID lens loaded MIMO antenna system is shown in inset of Fig. 14(a), wherein the size of the lens along  $z$ -axis is only modified to easily cover all six antenna elements. The modified dimensions of the GID lens are  $119 \times 35 \times 140 \text{ mm}^3$ . As shown in Fig. 14(a), the accepted -10 dB FBW of each antenna element with and without the lens is 9.3% (2.888–3.170 GHz) and 10.1% (2.884–3.190 GHz), respectively. It can be seen that at around 3.016 GHz the port-isolation ( $S_{21}$ ,  $S_{43}$ ,  $S_{65}$ ) after using the lens is significantly improved from 13.5 to 45 dB by 31.5 dB.

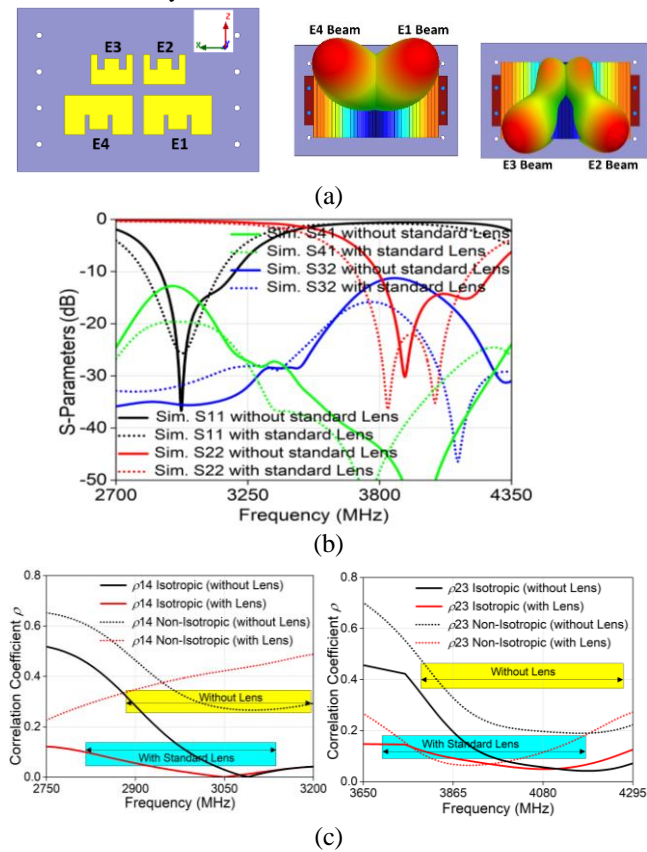


Fig. 15. (a) 4-element Multiband MIMO antenna with and without lens. (b)  $S$ -parameters. (c) Correlation Coefficient.

The simulated 2D normalized radiation patterns of all the six antenna elements in the  $xoy$ -plane with and without the GID lens are shown in Fig. 14(b). At 3 GHz, the beam maxima's of all the elements without the lens are slightly tilted to around  $\mp 29^\circ$ , whereas the tilt in beam maxima's with the lens for all elements remains the same except for E3 and E4 which is slightly reduced to  $\mp 25^\circ$ . The simulated gain and efficiency of each antenna element with (without) the lens within the desired FBWs are 3-4.16 dBi (2.3-3.8 dBi) and

48.6%-55.2% (44.8%-53.1%), respectively, which as compared to the previous case indicates improvement after using the lens. It can also be seen from Fig. 14(b), that there is no backward radiation degradation after using the lens except for E3 and E4. The  $\rho$  of the 6-element MIMO antenna configuration before and after using the GID lens in the isotropic environment only is shown in Fig. 14(c). This is because all the correlation coefficients have similar trend curves as compared to  $\rho$  of E-plane coupled 2-elements MIMO antenna example. The  $\rho$  for isotropic environment decreases from around 0.242 to 0.05 after using the lens. Similarly, the decrease in  $\rho_{12}/\rho_{34}/\rho_{56}$  is due to the radiation pattern spatial overlap reduction which can be credited to improvement in gain.

### C. MULTIBAND AND ULTRA-WIDEBAND MIMO ANTENNA

The proposed technique can be applied to antenna elements with a much wider operating bandwidth due to the dispersion free characteristics of the GID lens. The homogeneous permittivity value of each unit cell of the GID lens is designed using effective medium theory, according to which the unit cell size must be much smaller than the operating wavelength, *i.e.* smaller than  $1/5$  wavelength [30]. For this reason, the periodicity of 5 mm considered in this work relates to  $1/5$  wavelength of 12 GHz, which shows that the proposed lens can work up to X band frequency range.

To validate this point, three additional examples of the field decorrelation using the GID lens above the 4-element E shaped patch-based MIMO antenna (arranged in a  $2 \times 2$  configuration) operating at two different discrete frequency bands, a wideband 2-element U-Slot patch-based MIMO antenna and an ultra-wideband aperture coupled stacked 2-element patch-based MIMO antenna are considered, as shown in Figs. 15-17. In the first case shown in Fig. 15, a multiband response is achieved with a FBW of more than 10.3% at each discrete frequency band along with more than 8 dB port-isolation enhancement when same permittivity profile distribution standard GID lens of Fig. 5(e) is used with reduced unit cell dimensions of  $3 \times 3 \times 60 \text{ mm}^3$ . Moreover, Fig 15(c) shows  $\rho_{14}/\rho_{23}$  reduction for both isotropic and non-isotropic propagation environments when the antenna elements are loaded with GID lens. Similarly, in the second and third cases, a FBW of 20% and 33% is achieved with tilted patterns using the GID lens which not results in  $\rho$  reduction for both propagation environments but also enhances the port-isolation by more than 7 dB and 10 dB, as shown in Fig. 16(b) and Fig. 17(b), respectively. Even though 7 dB port-isolation enhancement is achieved when the modified GID lens is used in case of U-Slot patch-based MIMO antenna, the change in  $\rho$  with the modified GID lens is insignificant as compared to standard GID lens. This again reaffirms that further increase in port-isolation cannot guarantee  $\rho$  reduction for both isotropic and non-isotropic propagation environments.

Nevertheless, it is worthwhile to mention that the same standard GID lens is used efficiently for different antenna types working over various frequency bands with different

edge to edge spacing ( $0.06\lambda$  at 3 GHz,  $0.0083\lambda$  at 3 GHz,  $0.2\lambda$  at 11 GHz,) without varying the lens properties. However, this is not the case with the modified GID lens where the dielectric block dimensions in each case need to be optimized to get the maximum port-isolation enhancement. Most of the decoupling techniques not only lack this feature but also unable to simultaneously control the electromagnetic waves propagation and surface waves efficiently.

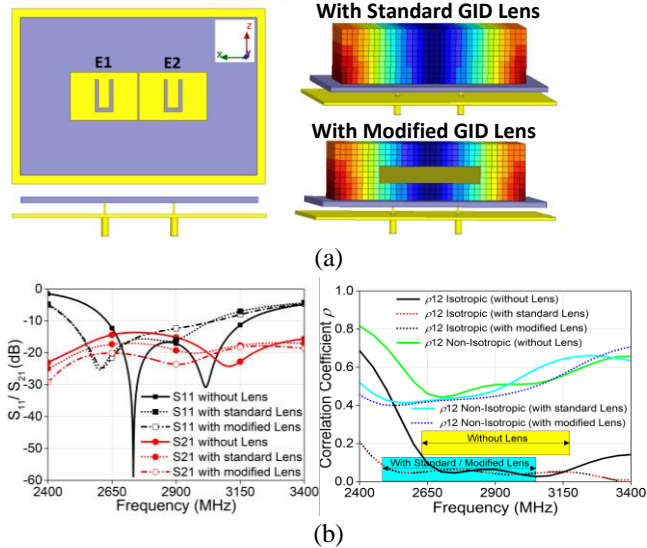


Fig. 16. (a) 2-element U-slot MIMO antenna with and without lens. (b)  $S$ -parameters and Correlation Coefficient.

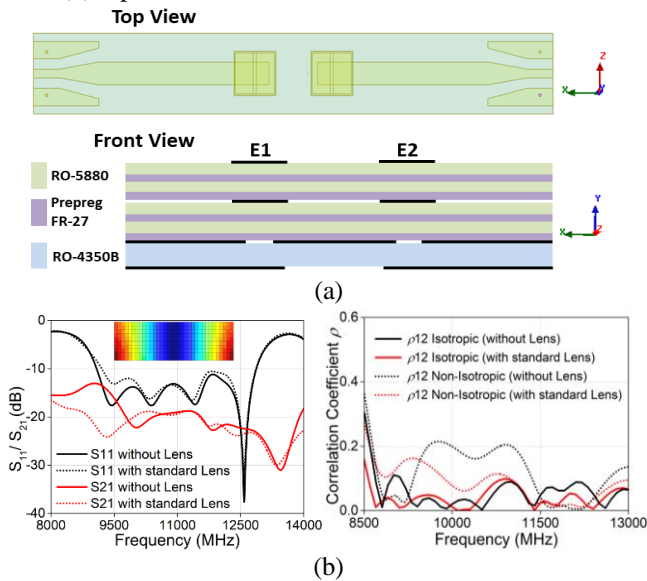


Fig. 17. (a) 2-element Stacked MIMO antenna with and without standard lens. (b)  $S$ -parameters and Correlation Coefficient.

#### D. COMPARISON WITH PREVIOUS WORKS

Table-I presents the performance comparison of the proposed method with some previous reported works on field decorrelation and decoupling. It is evident that for closely spaced antenna elements the proposed broadband GID lens not only enhances the port-isolation without reducing the FBW but can also reduce the  $\rho$  for both isotropic and non-isotropic

propagation environments by antenna beam tilting, which in all other decoupling designs [12-21] is not possible without employing microwave phase shifters. The PCE in [3] can effectively reduce the  $\rho$  of the narrow band MIMO antenna elements but the total efficiency remains low due to high mutual coupling. In [4], a combination of PMS and ADS is used to simultaneously achieve the decorrelation and decoupling of the narrow band MIMO antenna elements. Furthermore, most of the decoupling techniques reported in literature [8-20] have narrow operating bandwidth of less than 6.1% and are only effective for patch antenna elements arranged in either E-plane or H-plane orientation, but not both

Table-I. Comparison with previous reported works.

Ref	H/ E- Ports	Edge Spac.	IE dB	FBW	FBW Red.	PE
[3]	H - 4	0.063 $\lambda$	2	2%	No	Both Iso. & Non- Iso.
	H - 8		-3			
[4]	H - 4	0.2 $\lambda$	13	2.6%	No	Non- Iso.
[8]	H - 2	0.13 $\lambda$	-3	3%	Yes	Iso.
[9]	E - 6	0.35 $\lambda$	12	3.4%	Yes	Iso.
[12]	E - 2	0.42 $\lambda$	35	1.5%	No	Iso.
[17]	E - 2	0.12 $\lambda$	55	1.2%	No	Iso.
[18]	H - 2	0.03 $\lambda$	35	1.4%	No	$\rho$ not evaluated
[20]	H - 2	0.024 $\lambda$	12	6.1%	Yes	$\rho$ not evaluated
	E - 2	0.024 $\lambda$	15	5.8%		
	H - 8	0.028 $\lambda$	10	0.4%		
[21]	E-2	0.1 $\lambda$	43.9	14%	Yes	Iso.
	H-2	0.027 $\lambda$	20.6	27.3%		
PW	H - 2	0.1 $\lambda$	25	8.5%	No	Both Iso. & Non- Iso.
	E - 2	0.1 $\lambda$	32	10.1%		
	E - 6	0.1 $\lambda$	30	9.3%		
	H - 4	0.06 $\lambda$	8	10.3%		
	H - 2	0.008 $\lambda$	7	20%		
	H - 2	0.2 $\lambda$	10	33%		

PW.: Proposed Work, Spac.: Spacing, Red.: Reduction, IE: Isolation Enhancement, PE.: Propagation Environment. Iso.: Isotropic

planes except for [20-21], which may limit the utilization of these structures. Most importantly, such decoupling solutions cannot guarantee  $\rho$  reduction especially for non-isotropic environment. Also, such techniques turn back the beam maximum to the boresight direction [20-21], which afterwards increases the  $\rho$  in non-isotropic environment due to large 3D radiation pattern spatial overlapping. The wideband patch elements used in [20] and [21], have a reduction of fractional bandwidth when either a near-field resonator (NFR) or a dielectric block (DB) was placed above the antenna elements. This was due to the fact that the proposed NFR and DB in that work was only effective for the patch's basic resonant mode  $TM_{01}$ , but not  $TM_{02}$ . Also, the wideband field decorrelation of E-shaped patches cannot be achieved using the NFR, as  $\rho$  results was not provided in that work. In comparison, our proposed method has much wider usability (maximum of 33% FBW is achieved in one of the examples presented here) and intrinsic wideband phase matching at the interfaces for different antenna types working at different frequency bands as can be seen from Table-I. This feature is not being achieved by any previously reported work on field decorrelation and decoupling. Hence, the proposed technique provides a unique solution, which exploits the space deformation not only to decouple the adjacent antenna elements ports coupled in both planes but also to guarantee field decorrelation.

## V. CONCLUSION

In this paper, using a graded index all-dielectric lens, we have presented a new technique to simultaneously achieve the field decorrelation and decoupling of a closely spaced wideband coupled MIMO antenna elements arranged in two different orientations. By judiciously varying the permittivity profile of the GID lens using the concept of transformation electromagnetics, field decorrelation for  $\rho$  reduction is realized by tilting the radiation patterns of the antenna elements in opposite directions and, decoupling for mutual coupling reduction is achieved by suppressing the surface wave propagation in the antenna substrate. Besides, a wide FBW of minimum 8.5% and maximum of 33% is obtained for different decoupled MIMO antennas examples with the GID lens, respectively. Measured results after using the GID lens also reveals slight improvement in gain and radiation efficiency with almost no extra backward radiation. The proposed technique also has wider usability as same lens with a slight adjustment, either in dielectric slab dimensions or unit cell size, can be applied to wideband MIMO antennas working at different frequency bands.

## REFERENCES

- [1] A. J. Paulraj, D. A. Gore, R. U. Nabar and H. Bolcski, "An overview of MIMO communications - a key to gigabit wireless," in *Proc. of the IEEE*, vol. 92, no. 2, pp. 198-218, Feb. 2004.
- [2] R. G. Vaughan and J. B. Andersen, "Antenna diversity in mobile communications," *IEEE Trans. Vehicular Technol.*, vol. 36, no. 4, pp. 149-172, Nov. 1987.
- [3] M. Li, X. Chen, A. Zhang, A. A. Kishk and W. Fan, "Reducing Correlation in Compact Arrays by Adjusting Near-Field Phase

- Distribution for MIMO Applications," *IEEE Trans. Vehicular Technol.*, vol. 70, no. 8, pp. 7885-7896, Aug. 2021.
- [4] X. Chen et al., "Simultaneous Decoupling and Decorrelation Scheme of MIMO Arrays," *IEEE Trans. Vehicular Technol.*, vol. 71, no. 2, pp. 2164-2169, Feb. 2022.
- [5] S. Blanch, J. Romeu and I. Corbella, "Exact representation of antenna system diversity performance from input parameter description," *Electron. Lett.*, vol. 39, no. 9, pp. 705-707, 1 May 2003.
- [6] M. S. Sharawi, "Current misuses and future prospects for printed multiple-input multiple-output antenna systems," *IEEE Antennas Propag. Mag.*, vol. 59, no. 2, pp. 162-170, Apr. 2017.
- [7] S. M. Mikki and Y. M. M. Antar, "On cross correlation in antenna arrays with applications to spatial diversity and MIMO systems," *IEEE Trans. Antennas Propag.*, vol. 63, no. 4, pp. 1798-1810, Apr. 2015.
- [8] T. Hassan, M. U. Khan, H. Attia and M. S. Sharawi, "An FSS Based Correlation Reduction Technique for MIMO Antennas," *IEEE Trans. Antennas Propag.*, vol. 66, no. 9, pp. 4900-4905, Sept. 2018.
- [9] G. Das, A. Sharma, R. K. Gangwar, and M. S. Sharawi, "Performance improvement of multiband MIMO dielectric resonator antenna system with a partially reflecting surface," *IEEE Antennas Wireless Propag. Lett.*, vol. 18, no. 10, pp. 2105-2109, Oct. 2019.
- [10] G. Das, N. K. Sahu, A. Sharma, R. K. Gangwar and M. S. Sharawi, "FSS-Based Spatially Decoupled Back-to-Back Four-Port MIMO DRA With Multidirectional Pattern Diversity," *IEEE Antennas and Wireless Propag. Lett.*, vol. 18, no. 8, pp. 1552-1556, Aug. 2019.
- [11] X. Chen, S. Zhang, and Q. Li, "A review of mutual coupling in MIMO systems," *IEEE Access*, vol. 6, pp. 24706-24719, 2018.
- [12] K. Wei, J. Li, L. Wang, Z. Xing and R. Xu, "Mutual Coupling Reduction by Novel Fractal Defected Ground Structure Bandgap Filter," *IEEE Trans. Antennas Propag.*, vol. 64, no. 10, pp. 4328-4335, Oct. 2016.
- [13] S. Hwangbo, H. Y. Yang and Y. Yoon, "Mutual Coupling Reduction Using Micromachined Complementary Meander-Line Slots for a Patch Array Antenna," *IEEE Antennas Wireless Propag. Lett.*, vol. 16, pp. 1667-1670, 2017.
- [14] J. OuYang, F. Yang and Z. M. Wang, "Reducing Mutual Coupling of Closely Spaced Microstrip MIMO Antennas for WLAN Application," *IEEE Antennas Wireless Propag. Lett.*, vol. 10, pp. 310-313, 2011.
- [15] S. Ghosh, T. Tran and T. Le-Ngoc, "Dual-Layer EBG-Based Miniaturized Multi-Element Antenna for MIMO Systems," *IEEE Trans. Antennas Propag.*, vol. 62, no. 8, pp. 3985-3997, Aug. 2014.
- [16] Z. Qamar, L. Riaz, M. Chongcheawchamman, S. A. Khan, and M. F. Shafique, "Slot combined complementary split ring resonators for mutual coupling suppression in microstrip phased arrays," *IET Microw., Antennas Propag.*, vol. 8, no. 15, pp. 1261-1267, 2014.
- [17] A. Jafargholi, A. Jafargholi and J. H. Choi, "Mutual Coupling Reduction in an Array of Patch Antennas Using CLL Metamaterial Superstrate for MIMO Applications," *IEEE Trans. Antennas Propag.*, vol. 67, no. 1, pp. 179-189, Jan. 2019.
- [18] H. Qi, L. Liu, X. Yin, H. Zhao and W. J. Kulesza, "Mutual Coupling Suppression Between Two Closely Spaced Microstrip Antennas With an Asymmetrical Coplanar Strip Wall," *IEEE Antennas Wireless Propag. Lett.*, vol. 15, pp. 191-194, 2016.
- [19] H. Qi, X. Yin, L. Liu, Y. Rong and H. Qian, "Improving Isolation Between Closely Spaced Patch Antennas Using Interdigital Lines," *IEEE Antennas Wireless Propag. Lett.*, vol. 15, pp. 286-289, 2016.
- [20] M. Li, B. G. Zhong and S. W. Cheung, "Isolation Enhancement for MIMO Patch Antennas Using Near-Field Resonators as Coupling-Mode Transducers," *IEEE Trans. Antennas Propag.*, vol. 67, no. 2, pp. 755-764, Feb. 2019.
- [21] M. Li, M. Y. Jamal, L. Jiang and K. L. Yeung, "Isolation Enhancement for MIMO Patch Antennas Sharing a Common Thick Substrate: Using a Dielectric Block to Control Space-Wave Coupling to Cancel Surface-Wave Coupling," *IEEE Trans. Antennas Propag.*, vol. 69, no. 4, pp. 1853-1863, April 2021.
- [22] U. Qureshi, M. U. Khan, M. S. Sharawi, S. N. Burokur, and R. Mitra, "Field Decorrelation and Isolation Improvement in an MIMO Antenna using an All-Dielectric Device based on Transformation Electromagnetics," *Sensors*, vol. 21, no. 22, p. 7577, Nov. 2021.
- [23] M. Nikolic, A. Djordjevic, and A. Nehorai, "Microstrip antennas with suppressed radiation in horizontal directions and reduced coupling," *IEEE Trans. Antennas Propag.*, vol. 53, no. 11, pp. 3469-3476, Nov. 2005.

- [24] J. B. Pendry, D. Schurig, and D. R. Smith, "Controlling electromagnetic field," *Science*, vol. 312, no. 5781, pp. 1780–1782, Jun. 2006.
- [25] D. Schurig, J. B. Pendry, and D. R. Smith, "Calculation of material properties and ray tracing in transformation media," *Opt. Express*, vol. 14, no. 21, pp. 9794–9804, 2006.
- [26] H. F. Ma, T. J. Cui, "Three-dimensional broadband and broad-angle transformation-optics lens," *Nature Commun.*, vol. 1, pp. 124, Nov. 2010.
- [27] W. Tang, C. Argyropoulos, E. Kallos, W. Song and Y. Hao, "Discrete coordinate transformation for designing all-dielectric flat antennas," *IEEE Trans. Antennas Propag.*, vol. 58, no. 12, pp. 3795-3804, Dec. 2010.
- [28] J. Yi, S. N. Burokur, and A. de Lustrac, "Conceptual design of a beam steering lens through transformation electromagnetics," *Opt. Express*, vol. 23, no. 10, pp. 12 942–12 951, May 2015.
- [29] J. Li and J. B. Pendry, "Hiding under the carpet: A new strategy for cloaking," *Phys. Rev. Lett.*, vol. 101, p. 203901, Nov. 2008.
- [30] S. Xu, M. Zhang, H. Wen, and J. Wang, "Deep-subwavelength decoupling for MIMO antennas in mobile handsets with singular medium," *Sci. Rep.*, vol. 7, no. 1, p. 12162, Dec. 2017.
- [31] D. M. Pozar, *Microwave engineering*, 3rd ed. Hoboken, N.J.: Wiley, 2005.
- [32] Q. Wu, S. Guo and X. Chen, "Design of a low-profile antenna for use with 698-2700 MHz femtocell base stations," *IEEE Antennas Propag. Mag.*, vol. 60, no. 4, pp. 84-94, Aug. 2018.
- [33] M. P. Karaboikis, V. C. Papamichael, G. F. Tsachtsiris, C. F. Soras, and V. T. Makios, "Integrating compact printed antennas onto small diversity/MIMO terminals," *IEEE Trans. Antennas Propag.*, vol. 56, no. 7, pp. 2067-2078, 2008.
- [34] A. Ando, T. Taga, A. Kondo, K. Kagoshima and S. Kubota, "Mean Effective Gain of Mobile Antennas in Line-of-Sight Street Microcells With Low Base Station Antennas," *IEEE Trans. Antennas Propag.*, vol. 56, no. 11, pp. 3552-3565, Nov. 2008.
- [35] D. Sugimura, M. Arai, K. Sakaguchi, K. Araki, and T. Sotoyama, "A study on beam tilt angle of base station antennas for base station cooperation systems," in Proc. IEEE 22nd Int. Symp. Pers. Indoor Mobile Radio Commun., 2011, pp. 2374–2378.
- [36] M. S. Sharawi, "Printed multi-band MIMO antenna systems and their performance metrics," *IEEE Antennas Propag. Mag.*, vol. 55, no. 5, pp. 218-232, Oct. 2013.
- [37] C. Fager, X. Bland, K. Hausmair, J. C. Cahuana, and T. Eriksson, "Prediction of smart antenna transmitter characteristics using a new behavioral modeling approach," in *IEEE MTT-S Int. Microw. Symp. Dig.*, Jun. 2014, pp. 1–4.
- [38] D. R. Smith, S. Schultz, P. Markos, C. M. Soukoulis, "Determination of effective permittivity and permeability of metamaterials from reflection and transmission coefficients," *Phys. Rev. B*, vol. 65, 2002.
- [39] Ultimaker, "3D Printer Ultimaker 3 Specifications," *ultimaker.com*. <https://ultimaker.com/3d-printers/ultimaker-3> (accessed Feb. 10, 2021).
- [40] D.A. Ketzaki, and T.V. Yioultis, "Metamaterial-Based Design of Planar Compact MIMO Monopoles," *IEEE Trans. Antennas Propag.*, Vol. 61, no. 5, pp. 2758–2766, May 2013.



**Usman Qureshi** received the B.Sc. degree in Electrical Engineering from the University of Central Punjab, Pakistan, in 2011, and the M.S. degree in Electrical Engineering from the National University of Sciences & Technology, Pakistan, in 2020. He was the recipient of the 2008–2011 Pakistan Engineering Congress Scholarship for Graduate Engineering Studies. He is currently working in industry with a focus on antenna design and modelling. His current research interests include MIMO antenna, phased array antenna, All-dielectric graded index lens and integrated RF & Microwave subsystems.



**Muhammad Umar Khan** received the M.S. degree in electrical engineering from the GIK Institute of Engineering Sciences and Technology (GIKI), Topi, Pakistan, in 2008, and the Ph.D. degree in electrical engineering from the King Fahd University of Petroleum and Minerals (KFUPM), Dhahran, Saudi Arabia, in 2015. He is currently an Assistant Professor with the School of Electrical Engineering & Computer Science (SECS), National University of Sciences and Technology (NUST), Islamabad, Pakistan. His current research interests include printed antennas and antenna arrays, MIMO antenna systems, and reconfigurable antennas.



**Mohammad S. Sharawi** is a Professor (Professeur titulaire) of Electrical Engineering at Polytechnique Montréal, Montréal, Québec, Canada. He is also a member of the Poly-Grames Research Center at Polytechnique. He was with King Fahd University of Petroleum and Minerals (KFUPM), Saudi Arabia, between 2009-2018. He founded and directed the Antennas and Microwave Structure Design Laboratory (AMSDL) at KFUPM. He was a visiting Professor at the Intelligent Radio (iRadio) Laboratory, Electrical Engineering Department, University of Calgary, Alberta, Canada, during the Summer-Fall of 2014. He was a visiting research Professor at Oakland University during the summer of 2013. Dr. Sharawi's areas of research include Multiband Printed Multiple-Input-Multiple-Output (MIMO) Antenna systems, Reconfigurable and Active integrated Antennas, Millimeter-wave antennas, Integrated 4G/5G and beyond 5G antenna systems, Microwave sensors, Applied Electromagnetics, and computational methods. He has more than 370 papers published in refereed journals and international conferences, 11 book chapters (two of which in the *Antenna Handbook*, 5th edition, McGraw Hill, 2018), one single authored book entitled "Printed MIMO Antenna Engineering," Artech House, 2014, and the lead author of the recent book "Design and Applications of Active Integrated Antennas," Artech House, 2018. Dr. Sharawi has 28 issued/granted and 10 pending patents in the US Patent Office. He was the recipient of the Abdul Hameed Shoman Foundation Award (AHSF) for Arab researchers for the category of wireless systems in 2020 in addition to various best IEEE conference paper awards. Dr. Sharawi is serving as the Associate Editor for the IEEE Open Journal on Antennas and Propagation (OJAP), IET Microwaves, Antennas and Propagation (MAP), as well as an Area Editor (Antennas and Microwave Devices and Systems) for Wiley Microwave and Optical Technology Letters (MOP). He was an associate editor for IEEE Antennas and Wireless Propagation Letters (AWPL) from 2019-2023. Dr. Sharawi was the Specialty Chief Editor for the newly launched *Frontiers Journal on Communications and Networks* for the System and Test-Bed design section (2020-2022). He served on the Technical and organizational program committees as well as organized several special sessions on MIMO antenna systems and architectures in several international conferences such as EuCAP, APS, IMWS-5G, APCAP, iWAT among many others for many years. He is the IEEE Antennas and Propagation Society (APS) chair of the Montreal section as well as an active member of the IEEE Member benefits committee leading the initiative of the APS Student Travel grant. He is also the regional delegate of the EuRAAP in North America. Dr. Sharawi is currently a Distinguished Lecturer (DL) for the Antennas and Propagation Society (APS) during 2023-2025.



**Shah Nawaz Burokur** (M'98–SM'21) received the Ph.D. degree from Université de Nantes, Nantes, France, in 2005. He is currently an Associate Professor with Université Paris Nanterre, France. His current research interests are in the areas of microwave and applications of periodic structures, complex media, metamaterials, metasurfaces and metagratings, in the analysis of integrated planar and conformal circuits, antennas, sensors, orbital angular momentum and holographic imaging.

Dr. Burokur serves as an Editorial Board member and reviewer for various journals. On a national level in France, he is the co-coordinator of a think tank on new antenna concepts involving new technologies, such as metamaterials and metasurfaces, in the framework of the French GDR Ondes.



**Raj Mittra** (Life Fellow, IEEE) was a Professor in electrical and computer engineering with the University of Illinois at Urbana Champaign, Champaign, IL, USA, from 1957 to 1996. He was a Professor with The Pennsylvania State University, University Park, PA, USA. He has been a Visiting Professor with Oxford University, Oxford, England, U.K., and the Technical University of Denmark, Lyngby, Denmark. He is currently a Professor with the Electrical

Engineering Department, University of Central Florida, Orlando, FL, USA, where he is the Director of the Electromagnetic Communication Laboratory. He is also with Department of electrical and computer engineering, King Abdulaziz University, Jeddah, Saudi Arabia.

Dr. Mittra was a recipient of the Guggenheim Fellowship Award in 1965, the IEEE Centennial Medal in 1984, the IEEE Millennium Medal in 2000, the IEEE/AP-S Distinguished Achievement Award in 2002, the Chen-To Tai Education Award in 2004, the IEEE Electromagnetics Award in 2006, and the IEEE James H. Mulligan Award in 2011. He served as an Editor for the IEEE TRANSACTIONS ON ANTENNAS AND PROPAGATION. He is currently serving as the Co-Editor-in-Chief of the e-journal *Forum for Electromagnetic Research Methods and Application Technologies* (FERMAT). He is the Past-President of the IEEE Antennas and Propagation Society (AP-S).